5.1. Materials

Table 5.1: List of chemicals utilized while development of SSD-SLNs

S. No.	Materials	Suppliers
1	Silver Sulfadiazine	India Platinum Pvt. Ltd., Mumbai.
2	Compritol 888 Ato	Gattefosse Sas, France
3	Lutrol F 68	Basf, Germany
4	Potassium Dihydrogen Orthophosphate	Qualigens Fine Chemicals, Mumbai.
5	Di-Sodium Hydrogen Orthophosphate Anhydrous	Qualigens Fine Chemicals, Mumbai.
6	Polyethylene Glycol 600	Merck Limited, Mumbai
7	Acetic Acid For Hplc And Spectroscopy	S D Fine-Chem Limited, Mumbai.
8	Diethyl Ether Ar	S D Fine-Chem Limited, Mumbai.
9	Silver Sulfadiazine Cream Usp 1% W/W	Hind Pharma, Bhopal.
10	O-Phosphoric Acid	Spectrochem Pvt Ltd, Mumbai
11	Sorbitane Monooleate Lr	S D Fine-Chem Limited, Mumbai.
12	Chitosan	Sigma Aldrich, Bangalore, India
13	Liquor Ammonia (25%)	Thermo Fisher Scientific India Pvt. Ltd., Mumbai.
14	Type 1 Water	Arium® Pro Ultrapure Water Systems

5.2. Methods

5.2.1. Analytical method

5.2.1.1. Calibration curve of SSD in water

Stock solution (100 µg/mL) of the drug was prepared by dissolving 10 mg accurately weighed SSD in 25 µL of 25% ammonium hydroxide and then made up to 100 mL with type 1 water. From the stock solution, 0.5, 1, 2, 3, 4, 5 and 6 mL solutions were

taken out by pipette and diluted up to 50 mL with distilled water to finally obtain the concentrations of 1, 2, 4, 6, 8, 10, and 12 µg/mL, respectively. These final solutions were analyzed by UV-Vis spectrophotometer at 256 nm.

5.2.1.2. Calibration curve of SSD in phosphate buffer pH 6.8

Calibration curve of SSD was prepared in phosphate buffer pH 6.8 to determine the concentration of drug in the *in vitro* release samples. The Stock solution (100 µg/mL) of the drug was prepared by dissolving 10 mg accurately weighed Silver Sulfadiazine in 50 µL of 25% ammonium hydroxide and then made up to 100 mL with Phosphate Buffer pH 6.8. From the stock solution 0.5, 1, 2, 3, 4 and 5 mL solutions were taken out by pipette and diluted up to 50 mL with Phosphate Buffer pH 6.8, to finally obtain the concentrations of 1, 2, 4, 6, 8 and 10 µg/mL, respectively. These final solutions were analyzed in UV-Vis Spectrophotometer at 256 nm. Intra and inter day precision was also determined.

5.2.2. Preparation of SSD-SLNs

A slightly modified double emulsification-sonication technique was employed to achieve the SSD-SLNs with predetermined characteristics. Precisely, three step procedure, consisting of formation of primary emulsion in first step followed by secondary emulsion in second step and dispersion of the secondary emulsion in cold water to precipitate the nanosized melt emulsion in third step, was performed. Initially, 100 µL w/o surfactant (span 80) was homogeneously mixed with lipid melt (Compritol 888 melt at 70°C). Subsequently, SSD solution in 25% v/v ammonia was instilled gradually in the lipid melt to achieve the w/o emulsion with constant sonication. After primary emulsion formation, Lutrol F 68 aqueous solution having specific concentration (% w/v) was heated above the melting point of the lipid (75°C) and poured gradually in the lipid melt with constant application of sonication to attain the

w/o/w emulsion. Eventually, the formed hot secondary emulsion was precipitated out using the cold distilled water (2±3°C) under slow stirring (200 rpm).

5.2.3. Design of formulation experimentation

The Box-Behnken response surface design was utilized to optimize the various process and formulation factors with the help of Design-Expert software (7.0.0, Minneapolis, USA). Various formulation and process factors and their levels selected to achieve the optimized SSD-SLNs with desired quality attributes are provided in the Table 5.2**.** As appended in the Table 5.3, Total 17 batches were obtained with the help of software having different set of levels for the each experimental batch.

Table 5.2: Identified independent variables with their levels used in Box–Behnken experimental design and the predicted and experimental response obtained.

Code	Independent variables	Levels		Optimized
		Low	High	level
A	Ultrasonication time (min)	5	15	13
B	Surfactant concentration (% w/v)	1.5	2.5	2.25
C	Drug: lipid	4:1	6:1	5.24:1

- ***Optimization of SSD-SLNs***

The experimental responses in terms of particle size and % entrapment efficiency for each experiment are listed in the Table 5.3. Using the design expert, obtained findings were further statistically evaluated based on the lack of fit test and model statistic data to determine the suitable model describing the suitability of the method used. Based on the analysis of the variance, a polynomial equation succinctly explaining the effect of variables on quality parameters was generated along with 3D response surface graph by Design Expert. At last, the data was further processed to predict the optimized levels of formulation and process variables. At the same time, the predicted formulation

response was also predicted for the obtained set of the optimized factor's level. Eventually, using the predicted values of variables optimized formulation was prepared and characterized.

5.2.4. Particle size, polydispersity index and zeta potential

The formulated SSD-SLNs were evaluated using the Delsa Nano C particle size analyzer (Beckman Coulter, USA) at 25°C temperature to find out the particle size, polydispersity index *(*PDI) and zeta potential (ZP) of SSD-SLNs suspension. Specifically, appropriately diluted SSD-SLNs aqueous suspension was filled in the respective cuvette specific for the PS and ZP measurement. Fundamentally, the dynamic light scattering and electrophoretic movement of charged particle under the applied electric field is the basic principle for measurement of PS and ZP, respectively (Singh, Dadhania et al. 2016).

5.2.5. Entrapment efficiency

Entrapment efficiency was calculated by UV spectrophotometric method (Shimadzu 1800, Tokyo, Japan) at 256 nm. The upper chamber of nanosep tube was filled with 500 µL of nanosuspension and centrifuged at 15000 rpm for 10 min (10^{o}C). The filtrate diluted appropriately and absorbance was recorded at 256 nm. Finally, the free drug concentration was determined using the calibration curve to calculate the % EE of the suspension by the following formula:

$$\%\boldsymbol{EE} = \frac{\boldsymbol{Total\ amount\ of\ SSD - \ Amount\ of\ drug\ in\ the\ supernatent}}{\textbf{Total amount of SSD}} \boldsymbol{X\ 100}$$

5.2.6. Scanning electron microscopy (SEM)

The SSD-SLNs were analyzed using the scanning electron microscope (ZEISS, EVO18, Germany) to assess the shape, surface morphology and also the actual particle

diameter of the optimized SSD-SLNs. Briefly, with the help of the micropipette, a drop of the SSD-SLNs suspension was dispersed on the glass slide and dried at room temperature to finally get the fine film. Successively, gold coating was applied on the dried thin film of SSD-SLNs in the gold sputter coater QUORUM (Q150R ES) operating at high vacuum to incorporate the conductivity on the particles surface and to improve its sensitivity. The gold coated samples were finally analyzed by SEM (Jain, Patil et al. 2012, Agrawal, Harde et al. 2013).

5.2.7. *In vitro* release study

The *in vitro* release behavior of the SSD-SLNs was evaluated by the modified dialysis bag method at specified conditions (Agrawal, Aqil et al. 2017, Agrawal, Singh et al. 2017). Precisely, SSD-SLNs dispersion equal to 5 mg SSD was filled in a pre-soaked cellulosic dialysis bag and tied tightly to prevent the leakage. Next, the air tight bag was submerged in 250 mL of pH 6.8 phosphate buffer supplemented with 0.5%w/v Tween 80 in 500 mL beaker and processed at 37±0.5°C with perpetual stirring (50 rpm). Quantity sufficient samples were collected from the release medium at specific time points and replenished by fresh medium for maintaining the sink condition. The collected samples were appropriately diluted prior to the UV spectrophotometric analysis at λ_{max} 256 nm and the observed UV absorbance was extrapolated to calculate the cumulative release of SSD. Moreover, the release data was further fitted in different models to understand the release kinetics and mechanism of drug release.

5.2.8. Fourier transform infrared spectroscopy (FT-IR)

FT-IR study was performed to analyze the possible physicochemical interaction amongst the various formulation components and the SSD (SHIMADZU, Model 8400S Tokyo, Japan). Precisely, various powdered samples including SSD, compritol 888 ATO, Lutrol F 68, and SSD-SLNs were thoroughly mixed with dried KBr and pressed

to form the pellet within the sample holder. The prepared pellet was irradiated and scanned from 4000 cm^{-1} to 400 cm^{-1} wave range to acquire the FT-IR spectra and obtained spectrum for each sample was compared to observe the loss or change in peaks (Patel, Gade et al. 2019, Patel, Tripathi et al. 2019).

5.2.9. Differential scanning calorimetric (DSC) study

The differential scanning calorimetric analysis of samples, including SSD, physical mixture and the SSD-SLNs, was conducted to extract the information regarding the physicochemical interaction and the crystallinity of the drug. Nearly 5 mg powdered samples sealed hermetically in an aluminum crimp cell scanned over the 0°C-400°C temperature range at the rate of 10°C/min in the presence of the nitrogen (purging rate of 25 mL/min) to get the DSC thermogram. Moreover, the empty aluminum pan was considered as reference. Finally, the information like melting enthalpy and melting points of the sample were observed to deduce the desired information (Jain, Sharma et al. 2013).

5.2.10. X-ray diffraction (XRD) study

The XRD, of the pure SSD, physical mixture of all the components and lyophilized SSD-SLNs powders, was performed for gathering the crystallographic information of the SSD and the entrapped SSD in the SLNs. The samples were attached on sample holder (0.2 mm thick standard quartz) and the intensity of the diffracted X-ray and the diffraction pattern was recorded at various angle of diffraction (2Ɵ) varying from 5-80° using X-ray diffractometer (Rigaku, MiniFlex 600). The detector DTEX Ultra with high resolution and scanning speed of 10°/min was used to collect the diffracted rays. Finally the spectra was drawn using the raw data and analyzed to obtain the desired evidence regarding the crystalline nature (Vijayakumar, Kumari et al. 2016).

5.2.11. Bacterial strain and growth conditions

A standard *Pseudomonas aeruginosa* PA01 (ATCC 15692) strain was collected from the Institute of Medical Sciences, Banaras Hindu University, Varanasi and cultured overnight in Luria Bertani (LB) (Pronadisa, Spain) liquid medium at 37°C. The cultured microbial cells were centrifuged further at 8000 ×g for 10 min to isolate the grown microbes and resuspended in the fresh medium. Finally, the growth of the microbes was confirmed by observing the absorbance at A_{550}.

5.2.12. Minimal inhibitory concentration (MIC) assays

The minimum concentration of the SSD required to completely inhibit the growth of microbes is termed as the minimum inhibitory concentration (MIC). The MIC of the different samples including the pure SSD, SSD+DNase-I, SSD-SLNs and SSD-SLNs+DNase-I were estimated according to Clinical and Laboratory Standards Institute guidelines on planktonic *P. aeruginosa* culture by two fold broth dilution method in the 96 well plates (Polystyrene, transparent, sterile, BRAND plates) (Xie, Zhu et al. 2011, Gade, Patel et al. 2019). In brief, the double dilution technique was employed to prepare the 100 µL test sample with concentration varying from 100, 50, 25, 12.5, 6.25, 3.125, 1.5625, and 0.7812 µg/mL (equivalent to SSD) in 96 well plate. Subsequently, 100 µL planktonic *P. aeruginosa* culture equivalent to 5×10^5 CFU/mL in LB culture medium was inoculated in the test sample and incubated for 48 h at 37°C. Finally, A_{550} absorbance (nm) was measured at three different time interval (24, 36 and 48 h) in SYNERGY/HTX Multi-mode reader (Biotek, USA) to determine the MIC value. Three different evaluation time points were selected to collect the evidence regarding time dependent effect of different treatments on MIC.

5.2.13. Anti-biofilm activity of SSD-SLNs

The anti-biofilm study was performed to evaluate the biofilm elimination potential of the SSD-SLNs against the established biofilm of the *P. aeruginosa*. Various treatment groups *viz.* SSD, DNase-I, SSD+DNase-I, SSD-SLNs and SSD-SLNs+DNase-I were tested on *P. aeruginosa* biofilms (Tré-Hardy, Vanderbist et al. 2008, Baelo, Levato et al. 2015). Concisely, the biofilm was developed on the peg lids using the 96 well plates containing 5×10^5 CFU/mL *P. aeruginosa* PAO1 suspension (200 µL) in LB medium. Bacterial suspension in 96 well plate was covered with peg lid and incubated for 48 h at 37°C in the static condition. After 48 h incubation, the peg lids were rinsed with phosphate buffer saline pH 7.4 to remove the loosely attached bacteria. The rinsing was repeated thrice. Subsequently, biofilm containing peg lids were covered on the 96-well plates containing 200 µL of different test groups (equivalent to18.75 µg/mL SSD) and incubated at 37°C. The treatment was continued for three successive doses at 0, 24 and 48 h and each day the medium containing the treatments was replaced with fresh plates. At the same time, the biofilm elimination at 24, 48 and 72 h was quantified in terms of % biofilm residue remaining after treatment at different evaluation time points. To determine the % biofilm residue, treated biofilm was sonicated in the fresh 200 µL LB medium using the 96 well plate to collect the live microbes and centrifuged at 3000 rpm to get the cells. Finally, the centrifuged cells were diluted appropriately and plated on the LB agar for the growth. After incubation the CFU was calculated and the % biofilm residue determined.

Furthermore, the antibiofilm study was supported qualitatively and quantitatively (Thickness) by confocal laser scanning microscopy of the biofilms. For this, 2 well plates were utilized to grow the biofilm on the cover slip in LB using the above mentioned procedure. The biofilm grown on the cover slip was treated with the

different treatment groups for 24 h. Subsequently after 24 h treatment, the biofilm was fixed with 4% paraformaldehyde and stained by SYTO 9 (6 μM) and propidium iodide (30 μM) of the LIVE/DEAD BacLight Bacterial Viability kit (Thermo Fisher, Bangalore, India). Thereafter, the processed and stained biofilms were evaluated under confocal scanning laser microscopy (ZEISS, Germany) at the scanning wavelengths of 560 and 488 nm. Moreover, to determine the thickness of biofilms Z-stack images of biofilm was acquired at 2.03 μm z step size. Zen lite software (Zen lite 2012) was used to process the images and determine the thickness.

5.2.14. Determination of toxicity on human dermal fibroblast

In vitro cytotoxicity of the prepared SSD-SLNs and other formulation was assessed by MTT (3-[4,5-dimethylthiazol-2-yl]-2,5-diphenyltetrazolium bromide) colorimetric assay against the human dermal fibroblast (HDF). Briefly, 2 x 10^5 HDF cells were mounted in 96 well tissue culture plates and treated with different treatment (SSD equivalent to 100, 50, 25, 12.5, and 6.25 μg/mL). After 24 h incubation with treatments, the cells were centrifuged and the recovered supernatant was incubated with 10% MTT for 3 h at 37°C. Subsequently, the insoluble blue formazan formed was collected and dissolved in DMSO to measure the absorbance at 550 nm using a microplate reader SYNERGY/HTX Multi-mode reader (Biotek) to find out the % cell viability (Kushwah, Katiyar et al. 2018).

5.2.15. Preparation of SSD-SLNs loaded chitosan gel

After the various characterizations of the SSD-SLNs, the optimized SSD-SLNs were successfully incorporated in the 1% w/v chitosan gel prepared in 0.5% v/v acetic acid (pH adjusted to the 7.0 using the NaOH). Precisely, the SSD-SLNs were dispersed homogeneously in the chitosan gel by continuously stirring the mixture with the help of glass rod for 20 min. Subsequently, the mixture was sonicated in bath sonicator for 10

min to eliminate the entrapped air bubbles. Finally, the DNase-I was mixed using the glass rod to achieve the SSD-SLNs+DNase-I rich chitosan gel.

5.2.16. Texture profile analysis (TPA)

Mechanical property such as hardness, adhesiveness and elasticity of the hydrogel are the essential quality attributes need to be evaluated to get the ideal and optimized hydrogel formulation. These mechanical properties were determined using the Texture Profile Analyzer (TA.XT plus Texture Profile Analyzer, Stable Micro Systems, UK) (Singh, Vuddanda et al. 2015) and mechanical properties were extrapolated from the resultant force–time plots.

5.2.17. In-vivo wound healing studies on rat model

The prepared hydrogel rich in different formulation was tested for the in-vivo burn wound healing on Wistar Albino rats (200-250 g). For this purpose, animals were divided into four groups (n=6); Group 1: diseased control, Group 2: 1% w/w marketed SSD cream, Group 3: SSD-SLNs rich chitosan gel and Group 4: SSD-SLNs chitosan gel supplemented with DNase-I. The animals were collected from the Animal House Facility, Institute of Medical Sciences, Banaras Hindu University, Varanasi, India. Initially, hairs at the lateral abdominal region were removed using the shaving kit to create the uniform burn wound and the rats were given the 24 h rest prior to the wound formation to recover the any skin injury caused during the shaving. After 24 h rests, using the hot cylindrical rod (20 mm diameter) burn wound were induced on the ether anesthetized animals. Precisely, cylindrical iron rod was heated on intense flame for 5 min and positioned on the shaved region of the rats for 10 sec. to inflict the wound. In succession, the rats were given the treatment according to the group after 24 h of the burn initiation. The treatment was applied topically on the burn wound area for 21 days and the wound healing process for different group was measured on day 7^{th}, 14^{th}, and

21st in terms of the % wound retraction with respect to the area of the burn on day 1. At the end of the day 21, the animals were killed and the histopathological evaluation of the wound area was conducted to assess the re-epithelialization pattern in the different treatment groups (Mitsunaga Junior, Gragnani et al. 2012, Pereira, Dos Santos et al. 2012). The % wound retraction was calculated using the following formula;

$$\%\ \textbf{wound retraction on day x} = \frac{(\boldsymbol{wound\ area\ on\ day\ zero - wound\ area\ on\ day\ x})}{(\boldsymbol{wound\ area\ on\ day\ 0})} \boldsymbol{X\ 100}$$

5.2.18. Statistical analysis

Software GraphPad Prism 5.0 (GraphPad Software Inc., San Diego, CA) was utilized for the statistical analysis of the findings.

5.3. Results and Discussion

5.3.1. Analytical method

The calibration curve is prepared to calculate the SSD concentration in in-vitro release samples and the determination of the entrapment efficiency. The UV calibration curve of the SSD was successfully prepared in water and phosphate buffer pH 6.8 with linearity 0.9992 and 0.9989 (R^2 value), respectively.

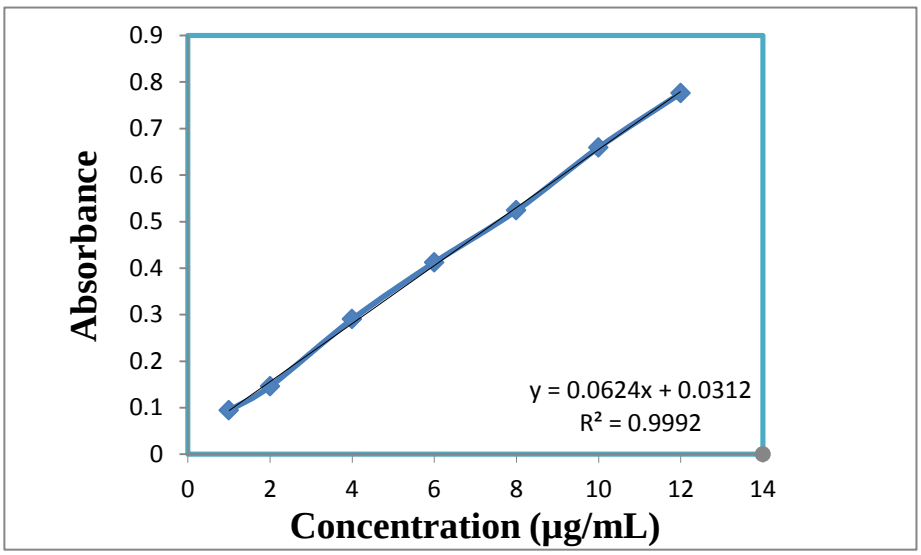

Figure 5.1: Calibration curve of SSD in water for UV spectrophotometry.

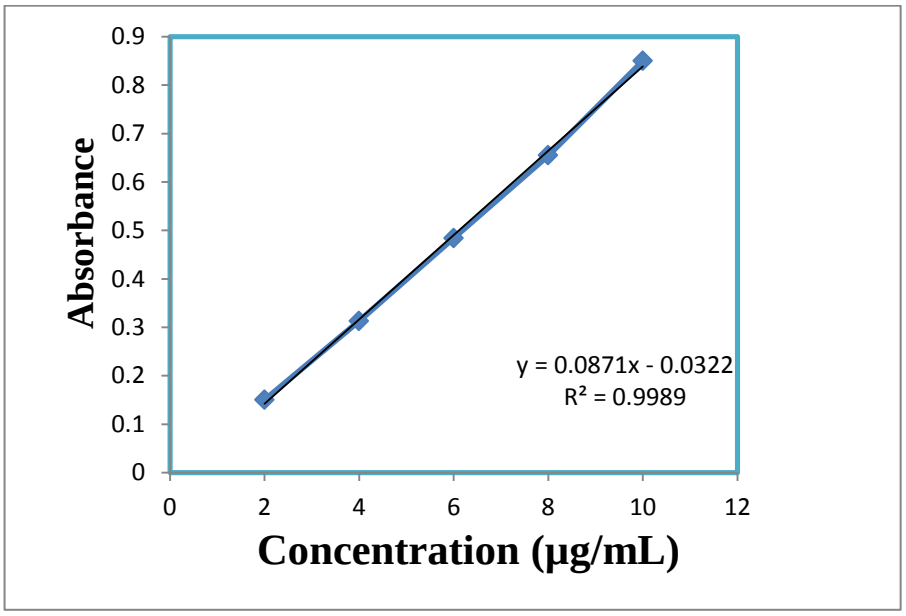

Figure 5.2: Calibration curve of SSD in phosphate buffer pH 6.8 for UV spectrophotometry.

5.3.2. Optimization of SSD-SLNs and analysis of variables

Exhaustive optimization of different critical parameters suggested that sonication time, surfactant concentration and lipid: drug ratio were the most influencing factors affecting the nanoformulation quality attributes. Surfactant plays a crucial role in particle stabilization by enveloping the film around the formed particles to achieve the stable and nano size particles. The response of the all the designed batches are presented in the Table 5.3. The SSD-SLNs were successfully optimized using the design of experiments approach and the optimized SSD-SLNs with obtained characteristics are depicted in Table 5.4. The statistical analysis of obtained findings related to PS and %EE was performed by analysis of variable which suggested that the quadratic model precisely demonstrates the effect of variables on PS and EE and was the best fit model.

Table 5.3: Complete experiment batches generated by software with their response.

S. no.	Ultrasonication time (min)	Sufactant Concentration (%w/v)	Lipid: Drig ratio	Particle Size (nm)	Zeta Potential (mV)
1	10	2.00	5:1	306.7	78.4
2	10	2.00	5:1	299.8	77.9
3	5	2.00	6:1	390.6	86.7
4	15	1.50	5:1	312.6	74.2
5	10	2.50	6:1	334.2	83.3
6	10	2.00	5:1	301.5	79.1
7	10	1.50	4:1	345.9	70.3
8	15	2.00	6:1	317.8	80.5
9	5	2.00	4:1	308.9	77.6
10	5	1.50	5:1	461.1	81.7
11	15	2.50	5:1	263.8	79.4
12	10	1.50	6:1	348.6	74.8
13	5	2.50	5:1	370.9	81
14	10	2.00	5:1	295.9	76.8
15	10	2.50	4:1	256.5	74.1
16	10	2.00	5:1	293.8	76.7
17	15	2.00	4:1	276.4	70.1

Table 5.4: Statistically predicted and empirically obtained PS and %EE of optimized SSD-SLNs.

		Responses	
S. No.	**Dependent variables**	**Predicted response**	**Experimental response**
1	Particle size (nm)	283.3	295.5±15.4
2	Entrapment efficiency (%)	79.2	75.9±3.4
3	PDI	-	0.261±0.023
3	Zeta Potential	-	-21.3±1.8

5.3.2.1. Effect of various factors on PS

The PS of the designed batches of SSD-SLNs ranged from 256.5±8.8 to 461.1±11.3 nm. The 3D surface plot was obtained from the software to explain the effect of variables on the PS. Moreover, the following polynomial equation generated by mathematical modeling or statistical analysis of the data demonstrated the effect of the lipid to drug ratio, sonication time and surfactant concentration on PS;

$$\boldsymbol{Particle\ Size} =$$

$$+299.54 - 45.11^{*}A - 30.35^{*}B + 25.44^{*}C + 10.35^{*}A^{*} - 10.08^{*}A^{*}C$$

$$+27.34^{*}A^{2} + 25.22^{*}B^{2} - 3.46^{*}C^{2} \quad \text{.....(1)}$$

The positive and negative signs in the equation denote the direct or inverse relation of variable effect, respectively, on PS. It is evident from the Figure 5.3A-5.3C and equation 1 that the sonication time, surfactant concentration and lipid to drug ratio, all had prominent effect on the PS, which described that small change in the said factors will significantly affect the PS. Sonication time with magnitude -45.11 and surfactant concentration with magnitude -30.35 shown to reduce the PS on increasing the levels. On contrary, upon increasing the lipid to drug ratio (+25.44) particle size was increased considerably.

5.3.2.2. Effect of variables on EE

Entrapment efficiency of SSD-SLNs batches varied from 70.3±5.1 to 86.7±6.5% (Figure 5.3D-5.3F). The polynomial equation 2 mentioned below illustrates the effect of different variables;

$$\%EE = +77.78 - 2.85^{*}A + 2.10^{*}B + 4.15^{*}C + 1.48^{*}A^{*}B + 0.32^{*}A^{*}C + 1.18^{*}B^{*}C$$

$$+2.20^{*}A^{2} - 0.90^{*}B^{2} - 1.25^{*}C^{2} \ldots\ldots\ldots\ldots\ldots\ldots\ldots\ldots\ldots\ldots\ldots\ldots\ldots\ldots\ldots\ldots (2)$$

Similar to our observation in PS, all the factors had the major role and affected the EE accordingly. The equation 2 depicting the effect of various factors on EE has magnitude

equal to -2.85, +2.10 and +4.15 for sonication time, surfactant concentration and lipid: drug ratio, respectively. The magnitude indicated that increase in sonication time resulted in the reduction in EE. However, surfactant concentration and lipid: drug ratio had favorable influence on the EE and upon increasing these factors the EE was also improved.

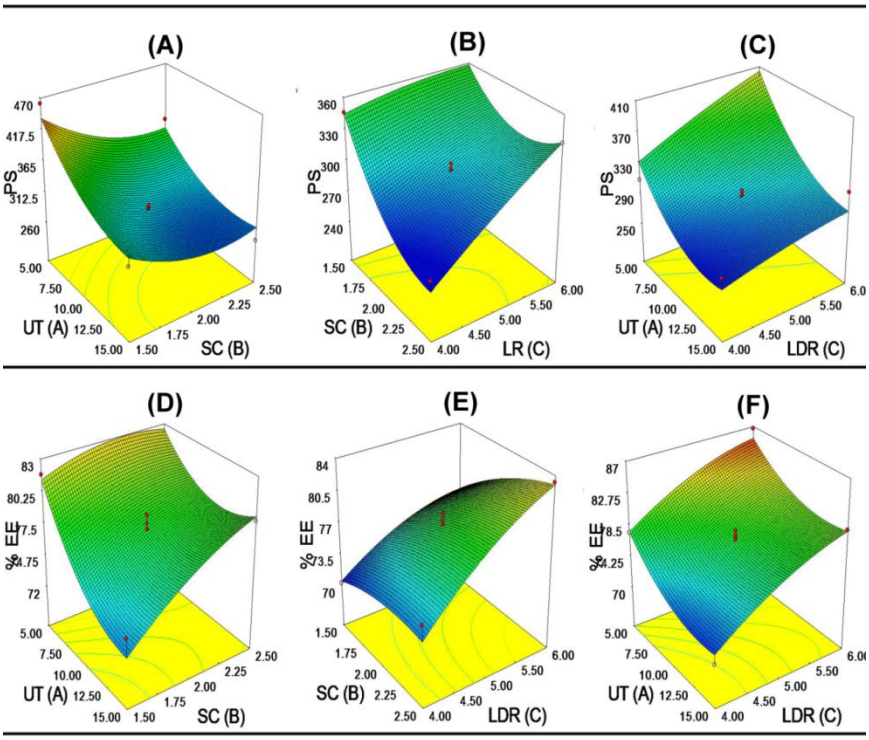

Figure 5.3: Software generated 3D plot expressing the effect of various factors on the PS and %EE.

5.3.3. Scanning electron microscopy (SEM)

The SEM image of SSD-SLNs (Figure 5.4) revealed spherical shape and uniform size distribution of the developed SLNs. Moreover, the particle size obtained by SEM (~ 300 nm) was approximately similar to the particle size measured by differential light scattering.

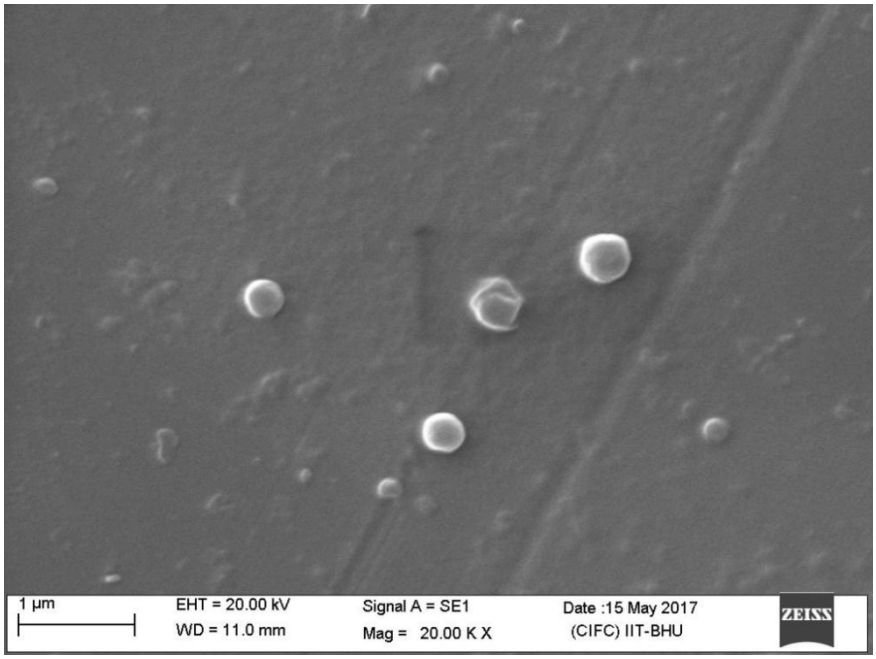

Figure 5.4: SEM micrograph of optimized SSD-SLNs.

5.3.4. In-vitro drug release study

SSD-SLNs showed initial burst release up to 35.3±3.9% in 3 h followed by sustained release up to 83.1±2.6% of SSD in 24 h (Figure 5.5). The kinetic evaluation of release data suggested that SSD-SLNs exhibited diffusion controlled release mechanism (followed Higuchi model; R^2 0.9686). Further, release kinetics suggested Higuchi model of drug release with R^2 0.9686 as a best fitted model to describe the SSD-SLNs release behavior (shown in Figure 5.5). The results were same as expected because the lipid matrix is hydrophobic, so the erosion of matrix in the buffer solution is supposed to be difficult. Hence, the release is possible only when medium diffuses to the matrix and dissolve the drug.

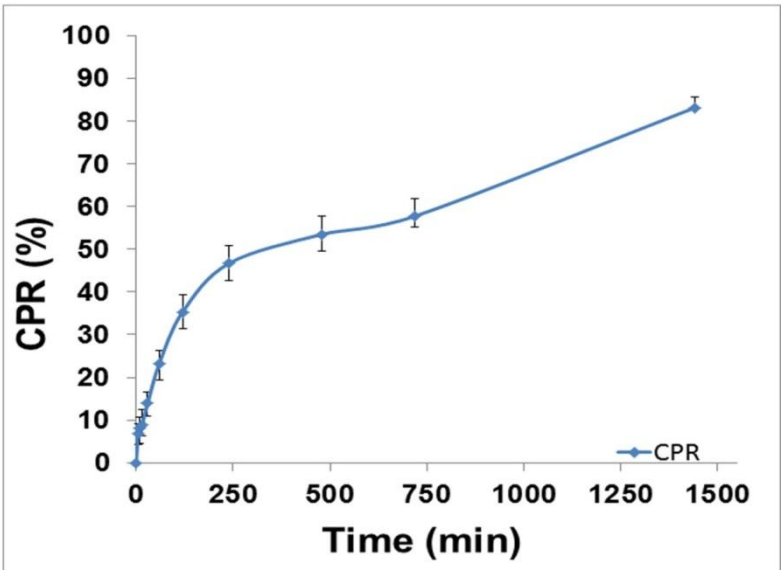

Figure 5.5: *In-vitro* drug release profile of SSD-SLNs in phosphate buffer pH 6.8 (mean±SD; n=3).

5.3.5. FT-IR

The physicochemical compatibility of SSD and excipients was studied using FT-IR analysis. The FT-IR spectra of SSD (Figure 5.7) depicted the specific and intense peaks at 3390.97, 3344.68 cm^{-1} (N-H stretching), 3074.63 cm^{-1} (aromatic =C-H stretching), 1654.98 cm^{-1} (N-H bending), 1599.04, 1581.68, 1552.75, 1500.67 cm^{-1} (aromatic C=C stretching), 1232.55 cm^{-1} (aromatic C-N stretching), 1356.00 cm^{-1} (S=O asymmetric stretching), and 1118.39 cm^{-1} (S=O symmetric stretching). Similarly, all these peaks were intact and present with minor or no transformation in intensity and position in the spectra obtained for SSD-SLNs. Findings revealed that, SSD and other components of the SSD-SLNs did not show any sign of potential physical or chemical interaction as most of the transmittance peaks specific to functional groups of SSD in FTIR spectra were also present in SSD-SLNs spectra (Figure 5.7).

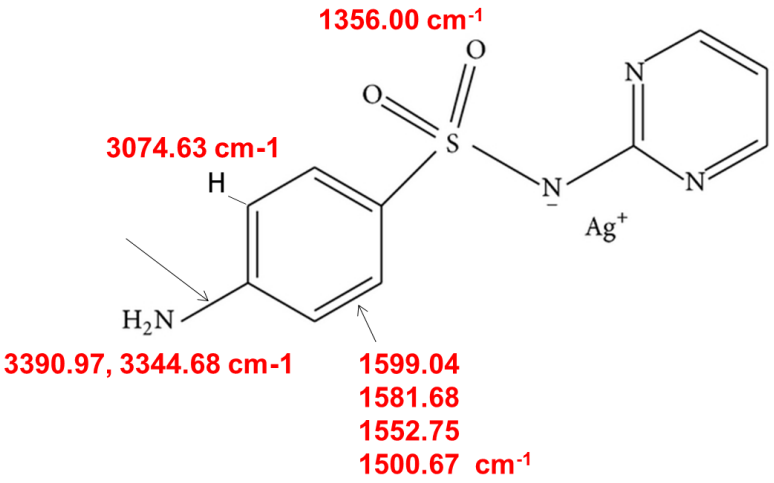

Figure 5.6: FT-IR peaks corresponding to the functional groups of the SSD

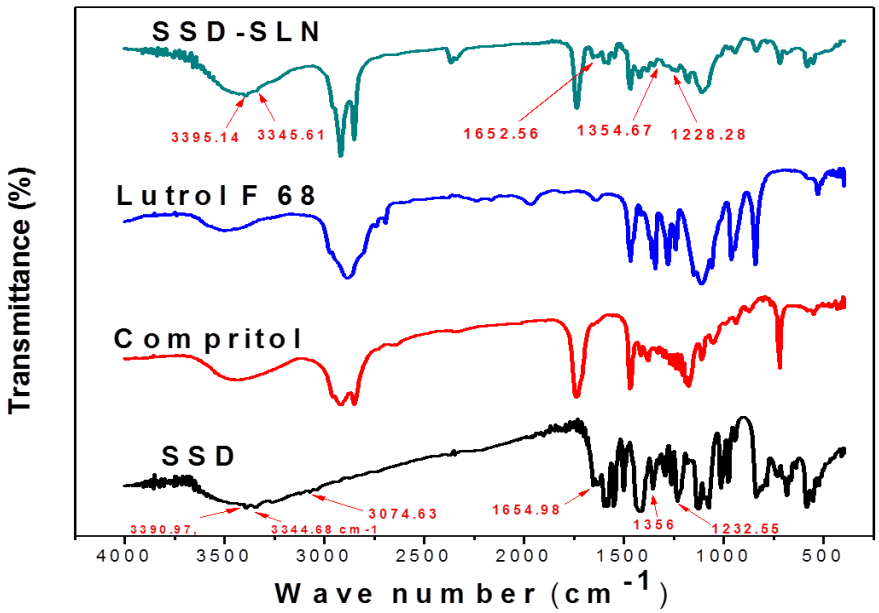

Figure: 5.7: Overlapped FT-IR spectrum of SSD, compritol 888 ATO, Lutrol F 68, and SSD-SLNs.

5.3.6. Differential scanning calorimetric study

The DSC thermogram (Figure 5.8) corresponding to pure SSD had a sharp endothermic peak at 286.56°C suggesting the crystalline nature of SSD. The crystalline behavior of SSD was well maintained in the physical mixture with insignificant shift in endothermic peak (282.90°C). Precisely, the minor shift in melting point peak indicated

the better compatibility and no interaction of SSD with excipients. However, thermogram for SSD-SLNs possessed endothermic peak at same melting point 286.56°C as SSD but with reduced and broadened peak intensity. Thus the unchanged position of the melting point of SSD in physical mixture and the SSD-SLNs show in DSC thermogram (Figure 5.8) confirmed the absence of interaction. However, loss or broadening of sharp endothermic peak in DSC thermogram indicated either the conversion of crystalline SSD to amorphous or a uniform molecular distribution in a solid matrix of lipids (Singh, Vuddanda et al. 2015)

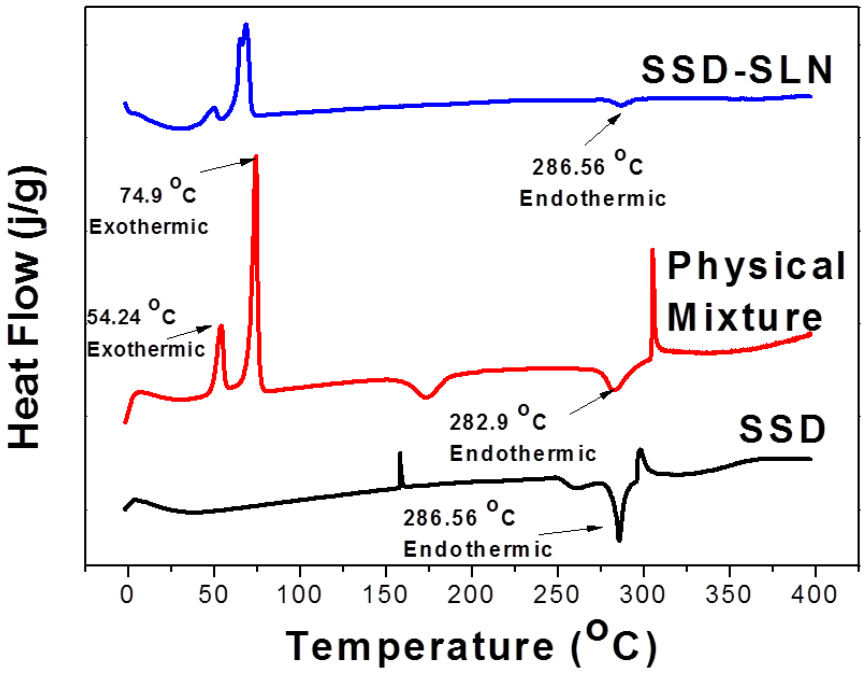

Figure 5.8: DSC thermograms of SSD, physical mixture and SSD-SLNs showing effect of excipients and formulation on melting of SSD.

5.3.7. XRD study

The diffraction pattern of SSD (Figure 5.9) demonstrated the complete crystalline behavior with many peculiar, intense and sharp peaks detected at 2θ of 8.77, 10.32, 16.21, 19.93, 24.5, 27.97, 33.13, 37.46, 38.65 and 40.82 and many more minor peaks

up to 60°. On contrary, most of these diffraction peaks were absent, deformed and broadened in the diffraction pattern of SSD-SLNs. Lost, deformed and blunted diffraction peaks in XRD spectra (Figure 5.9) indicated either the conversion of crystalline SSD to amorphous or a uniform molecular distribution in a solid matrix of lipids (Singh, Vuddanda et al. 2015).

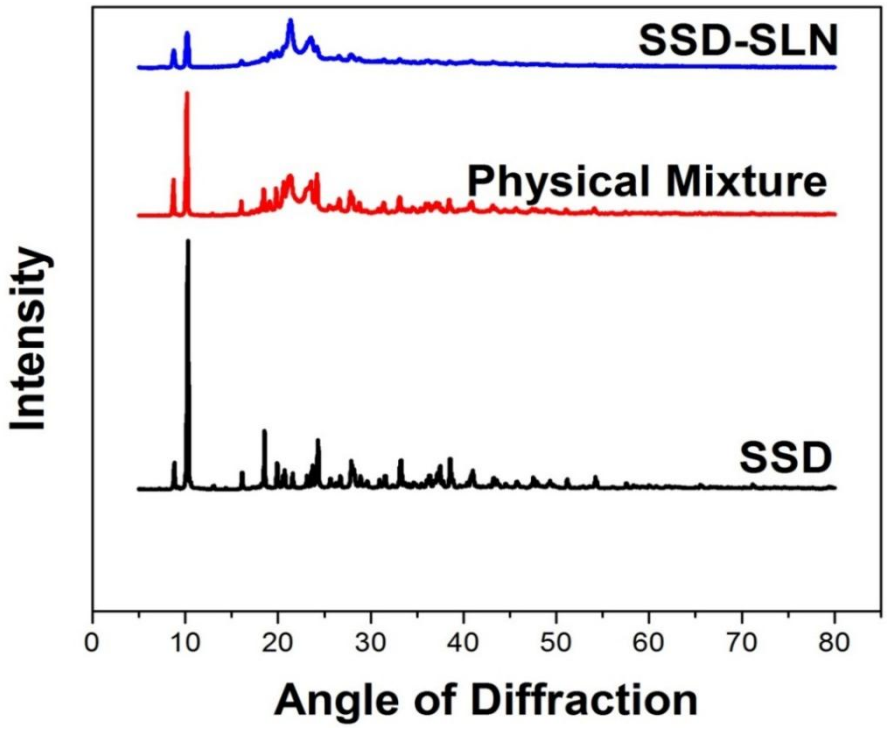

Figure: 5.9: X–ray diffraction patterns of SSD, physical mixture, and SSD-SLNs.

5.3.8. MIC determination

The results of *in-vitro* MIC studies (Table 5.5) elucidate that pure SSD and SSD-SLNs both had the same MIC (18.75 µg/mL) after 24 h. But after 24 h, MIC of pure SSD shifted to higher side from 18.75 to 25 µg/mL in a temporal manner during incubation. Besides that, SSD-SLNs had a constant MIC of 18.75 µg/mL at all-time points during incubation (24, 36 and 48 h). The observed phenomenon could be ascribed to the prolonged release of drug (Cheow, Chang et al. 2010, Wang, Hu et al. 2017) and enhanced fusion of SLNs to the bacterial membrane. The gradual enhancement in MIC

of the SSD may be ascribed to the sub therapeutic concentration of SSD or may be due to faster multiplication of bacteria escaped from drug action under adverse conditions (Xie, Zhu et al. 2011).

Table 5.5: MIC value of different formulations against *P. aeruginosa* and biofilm thickness treated with different formulations.

S. No.	Formulation	MIC (µg/mL) at different time (h)		
		24	**36**	**48**
1	Pure SSD	18.75	25	25
2	SSD+DNase-I	18.75	25	25
3	SSD-SLNs	18.75	18.75	18.75
4	SSD-SLNs+DNase-I	18.75	18.75	18.75

5.3.9. Anti-biofilm properties using repeated doses of treatment

This study was performed to evaluate the anti-biofilm potential of SSD-SLNs with or without DNase-I on 48 h grown *P. aeruginosa* biofilm *(*Figure 5.10). SSD-SLNs efficiently improved the antimicrobial activity against the planktonic as well as the established biofilm of the *P. aeruginosa* and strongly supported the proposed hypothesis. Three subsequent doses of SSD and SSD-SLNs without DNase-I could remove only 58.1 and 78.7% of biofilm after 72 h treatment, respectively. The antibacterial property of formulation enhanced significantly ($p<0.05$) following the addition of DNase-I with SSD and SSD-SLNs. Nevertheless, SSD-SLNs with DNase-I alone demonstrated significantly higher ($p<0.05$) eradication of the biofilm after 24, 48, and 72 h of treatment as compared to other treatment groups. SSD-SLNs exerted maximum anti-biofilm activity when combined with DNase-I, around 96.8% of biofilm was reduced after 3rd dosing (72 h) while, the SSD in combination with DNase-I could only reduce the 82.9% of biofilm (Baelo, Levato et al. 2015). The higher anti-biofilm efficiency of SSD-SLNs over the SSD may be attributed to the facilitated diffusion of

the SSD-SLNs in the porous matrix of the biofilm resulting in the delivery of drug to proximity of bacterial colony, thus improved the penetration of drugs in biofilm and enhanced antibacterial activity (Henning, Schneider et al. 2010, Jørgensen, Wassermann et al. 2013, Nafee, Husari et al. 2014). Though SSD-SLNs alone and pure SSD with DNase-I remarkably improved the annihilation of biofilm, the SSD-SLNs along with DNase-I possessed highest biofilm eradication potential thus prevailed the limitation of SSD therapy and biofilm resistance. The DNase-I hydrolyzes the eDNA in biofilm matrix and favor the mobility and distribution of SSD and SSD-SLNs in the biofilm. Conclusively, the findings of anti-biofilm evaluation suggested that SSD-SLNs along with DNase-I can easily penetrate into biofilm and may actively reduce the biofilm integrity and also kill the microbes. In fact, DNase-I disperse the ECM by degrading the eDNA of biofilm and breaking of eDNA molecules reduces the strength, make biofilm more permeable for antibiotics and improve the antibiotic's efficacy (Okshevsky, Regina et al. 2015). Furthermore, confocal evaluation of SYTO9/PI stained biofilms treated with different formulation also supported the findings of the anti-biofilm study (Figure 5.11.i-v). To support above results the biofilm thickness (Table 5.6) was determined using acquired Z-stack of scanned section of biofilm grown and treated on cover slips in 12 well culture plate using confocal laser scanning microscopy (CLSM).

The outcome revealed that apart from improved antibacterial activity, SSD-SLNs with DNase-I has also reduced the biofilm thickness, indicating the biofilm dispersal potential of DNase-I which increase the mobility and permeability of SSD-SLNs in biofilm. Confocal images (Figure 5.11i-5.11v) of biofilm treated with different groups clearly indicated the remarkable difference in the density of live and dead cell stained with Green SYTO9 and red Propidium iodide, respectively.

Table 5.6: The MBEC value of different formulation against the *P. aeruginosa* biofilm.

S. No.	Formulation	Biofilm thickness (µm) (mean ± S.D)
1	Untreated	63.2±5.9
2	Pure SSD	52.7±6.1
3	SSD+DNase-I	40.4±4.1
4	SSD-SLNs	45.8±3.9
5	SSD-SLNs+DNase-I	24.6±3.4 *

n=3; Values represent the mean ± S.D. One way ANOVA was performed (, P<0.05 vs SSD-SLN+DNase-I

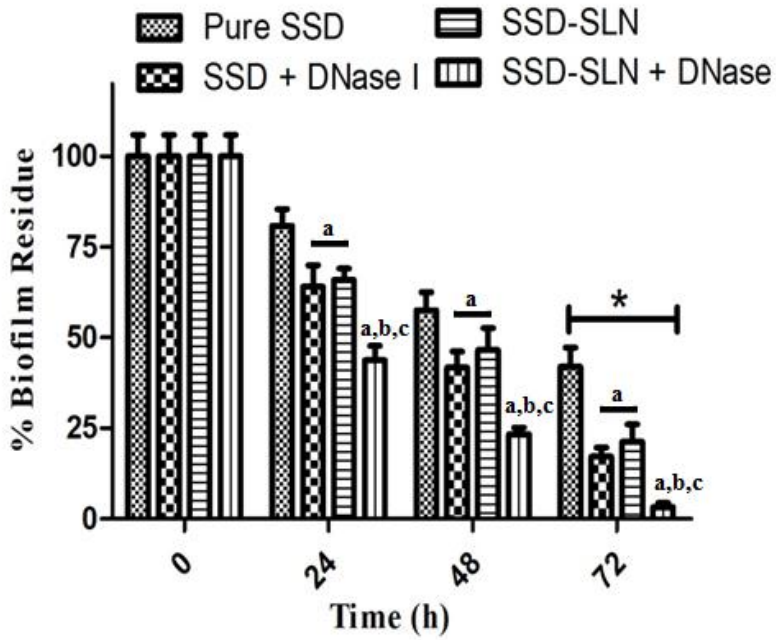

Figure 5.10: The graph indicates the comparative inhibition of established *P. aeruginoas* biofilm after three consecutive dosing (once a day) of pure SSD or encapsulated SSD (18.75 µg/mL) with or without DNase-I (20 µg/mL). A repeated measure two way ANOVA with bonferroni post hoc test was performed (^{a}P<0.05 comparison to pure SSD, ^{b}p<0.05 comparison to SSD-SLN, ^{C}p<0.05 comparision to SSD+DNase-I *p<0.05 group comparison at 0,24, 48 h (time variable). The viable counts $2.3 \times 10^{9} \pm 9.1 \times 10^{7}$ cfu/mL in untreated biofilm was taken as hundred percent. Data are in mean ± SD (N=3).

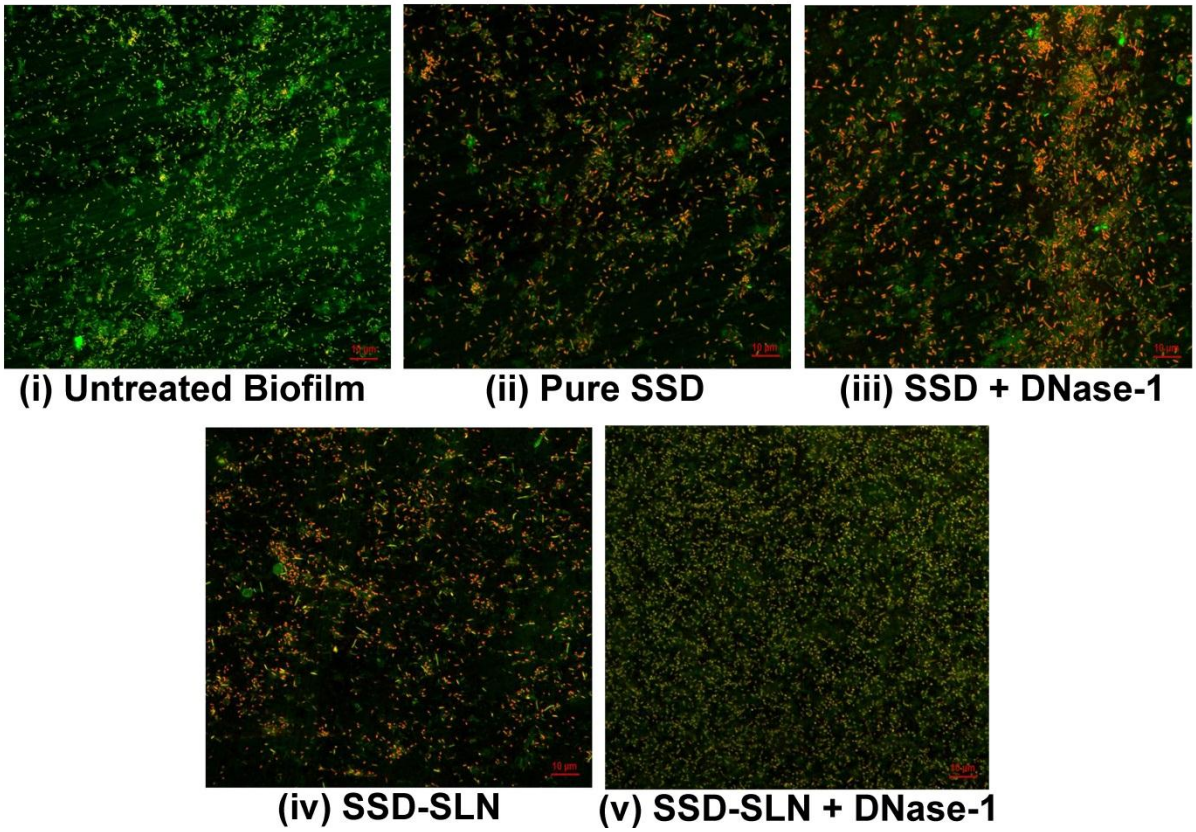

Figure 5.11: CLSM images of *P. aeruginosa* biofilm treated with different test samples (40X magnification). Green fluorescent (SYTO9) cell indicated the Live bacterial cell and red fluorescent (PI) for dead cell. **(i)** Untreated *P. aeruginosa* biofilm, **(ii)** pure SSD, **(iii)** SSD+DNase-I, **(iv)** SSD-SLNs **(v)** SSD-SLNs+DNase-I. (SSD equivalent to 18.75 µg/mL and DNase-I equivalent to 20 µg/mL).

5.3.10. Determination of toxicity on human dermal fibroblast

The results of MTT assay (Figure 5.12), revealed that SSD-SLNs demonstrated remarkably higher cytoprotective activity against HDF as compared to pure SSD and SSD with DNase-I. Pure SSD had dose-dependent toxicity on HDF in which 100 µg/mL of SSD exhibited 76.9±4.2% cell viability, whereas, the cell viability increased significantly ($P<0.05$) for SSD-SLNs (90.3±3.8% at 100 µg/mL). In addition, DNase-I with SSD and SSD-SLNs did not affect the cytotoxicity of SSD and SSD-SLNs significantly ($P>0.05$). The findings of MTT assay (Figure 5.12) unveiled that unlike the SSD, SSD-SLNs had significantly higher ($p<0.05$) cell viability which indicated the

decreased fibroblast toxicity and can be attributed to the encapsulation of SSD in SLNs, which prevented the direct exposure of high concentration of SSD to HDF (Sandri, Bonferoni et al. 2013).

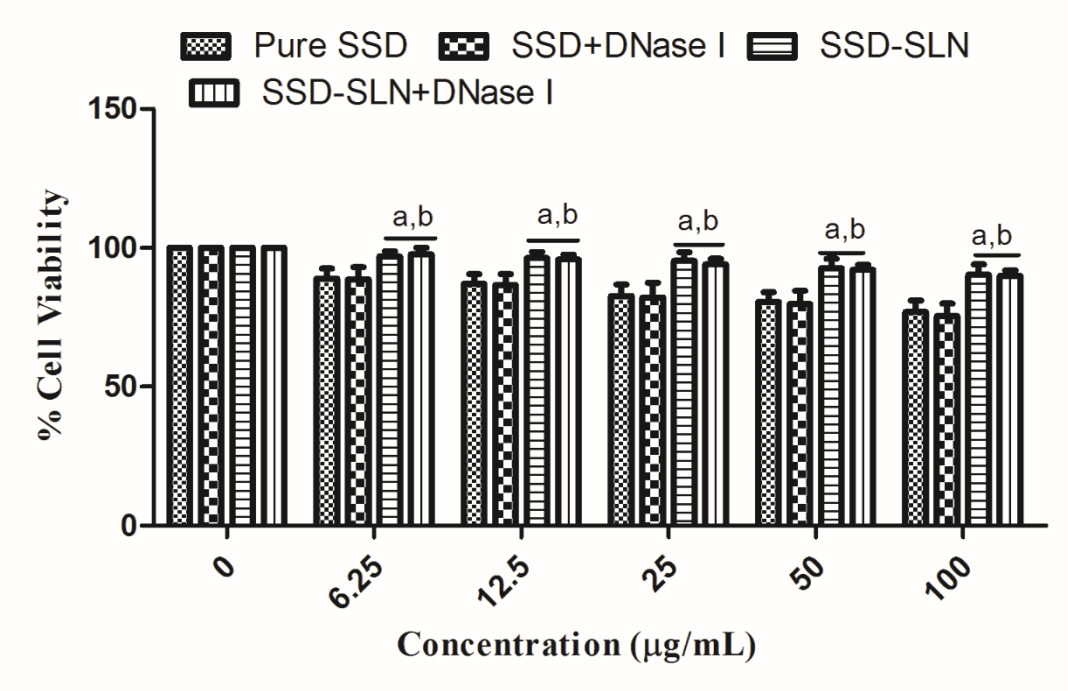

Figure 5.12: Bar graph represents the percentage viable dermal fibroblast incubated with varying concentration of pure and encapsulated SSD after 24 h. A repeated measure two way ANOVA was performed (a, $p<0.05$, vs pure SSD; b, $p<0.05$, vs SSD+DNase-I).

5.3.11. Texture Profile analysis

The SSD-SLNs were successfully incorporated in the chitosan gel and shown to have favorable mechanical properties (appended in Table 5.6) sufficient enough to achieve the good spreadability, sufficient surface adhesion and easy washing and might be ascribed to the accumulation of SSD-SLNs particles in 3D structure of chitosan gel (Garg and Singh 2014). Mechanical properties of hydrogels such as hardness, adhesiveness and elasticity were extrapolated from force-time plot. As mentioned in Table 5.6, the hardness, adhesiveness and elasticity of chitosan gel did not affect

significantly on incorporating SSD-SLNs in chitosan gel. Ideally the gel system should possess low hardness, high adhesiveness and moderate elasticity. Basically, low hardness supports the easy removal of gel, while the high adhesion offers the retention for longer duration. At the same time, moderate or high elastic modulus of the gel prevents the drug expulsion and improves the steady release pattern (Singh, Vuddanda et al. 2015). Low hardness, high adhesiveness and moderate elasticity of prepared SSD-SLNs chitosan gel provided the ideal formulation properties for wound dressing.

Table 5.6: Mechanical properties of different gel formulations.

Gel Parameters	**Blank Chitosan Gel** (mean ± SD*)	**SSD-SLN incorporated Chitosan gel** (mean ± SD*)
Hardness (N)	6.9±0.4	7.2±1.2
Adhesiveness (N-mm)	35.4±1.8	36.8±3.1
Elasticity (mm)	4.7±0.5	4.54±0.6

*n=3; Values represent the mean ± standard deviation.

5.3.12. Comparative wound healing Study

For comparative wound healing activity, the % burn area retraction on 7th, 14th and 21st day was compared with the burn area on 0 day along with the visual observation. Wound retraction in the untreated group and group 2 treated with marketed cream (50.3±2.3 and 76.3± 2.2 % burn retraction, respectively) was partial even after 21 days of treatment (Figure 5.13(i – ii) and Table 5.7). Interestingly, treatment with SSD-SLNs laden gel along with DNase-I displayed excellent wound healing property with 89.3± 3.1% wound area retraction on day 14 and produced the complete wound healing on day 21. SSD-SLNs treated group demonstrated 94.7± 3.1% wound area retraction on day 21. Furthermore, the histological images of sacrificed rat skin (Figure 5.13(iii, iv)) confirmed the faster and intact re-epithelialization by SSD-SLNs containing gel with

and without DNase-I. On contrary untreated animals (Figure 5.13i) and animals received marketed cream formulation (Figure 5.13ii) had damaged and incomplete re-epithelialization on day 21.

The faster and normal wound healing by SSD-SLNs loaded chitosan gel in combination to DNase-I may be attributed to the improved antimicrobial activity of SSD-SLNs with or without DNase-I. At the same time, DNase-I prevents the adherence and development of biofilm formation. Moreover, cytoprotective activity of SSD-SLNs against dermal fibroblast (Shown in MTT assay) further accelerates the wound healing (Sandri, Bonferoni et al. 2013). Finally, the histological evaluation of HE stained retracted wound skin revealed the intact and complete re-epithelialization of skin in case of SSD-SLNs and DNase-I rich chitosan gel treatment.

Table 5.7: Percent wound area retraction of rats in different groups with or without treatment. Value represents the average (mean ± SD) of % wound area of all animal in individual group.

Groups	**Treatment**	**% Wound retraction on different days** (mean ± SD*)			
		0 days	**7th Day**	**14th day**	**21st day**
Group 1	Untreated	0	15.5± 2.9	31.9± 1.9	50.3±2.3
Group 2	Marketed cream	0	31.8± 1.9	55.5± 3.4	76.3± 2.2
Group 3	SSD-SLN gel	0	45.4± 1.1	80.8± 4.2	94.7± 3.1
Group 4	SSD-SLN+DNase-I gel	0	48.9± 3.2	89.3± 3.1	100

*n=3; Values represent the mean ± standard deviation. SSD-SLN gel represents Silver sulfadiazine SLN loaded chitosan gel; SSD-SLN+DNase-I gel indicates Silver sulfadiazine SLN loaded chitosan gel incorporating DNase-I

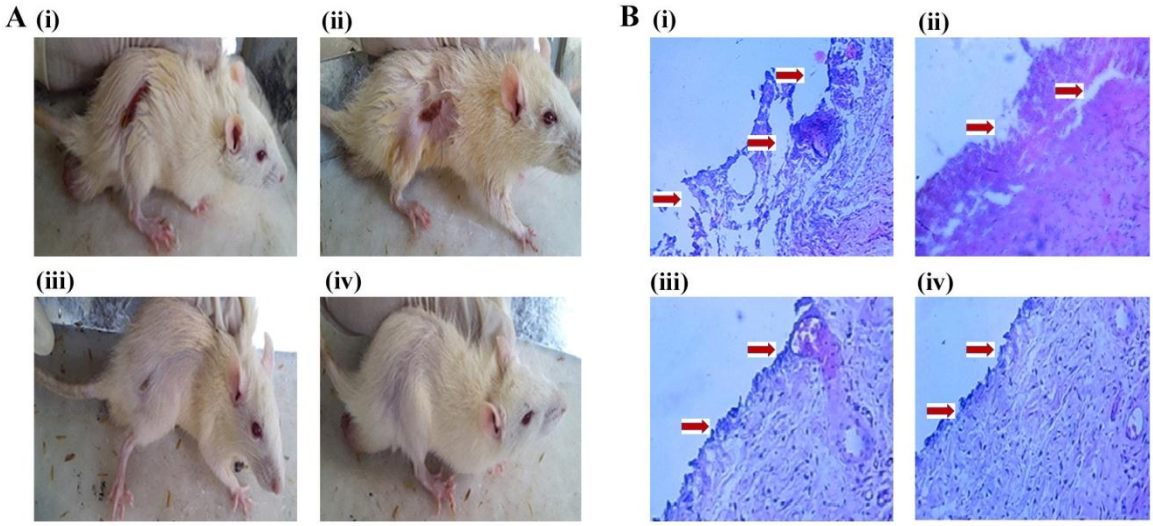

Figure 5.13: (A) Comparative burn wound healing images of rats after 21 days; & **(B)** Histopathology of re-epithelialized rat skin after 21 days treatment showing at 10X magnification; The treatment group includes: **(i)** Untreated (diseased control); **(ii)** SSD marketed cream; **(iii)** SSD-SLNs chitosan gel; **(iv)** SSD-SLNs+DNase-I chitosan gel.